

# EULERIAN-LAGRANGIAN RUNGE-KUTTA DISCONTINUOUS GALERKIN METHOD FOR TRANSPORT SIMULATIONS ON UNSTRUCTURED MESHES\*

XIAOFENG CAI<sup>†</sup> AND JING-MEI QIU<sup>‡</sup>

**Abstract.** Semi-Lagrangian (SL) approach is attractive in transport simulations, e.g. in climate modeling and kinetic models, due to its numerical stability in allowing extra-large time-stepping sizes. For practical problems with complex geometry, schemes on the unstructured meshes are preferred. However, accurate and mass conservative SL methods on unstructured meshes are still under development and encounter several challenges. For instance, when tracking characteristics backward in time, high order curves are required to accurately approximate the shape of upstream cells, which brings in extra computational complexity. To avoid such computational complexity, we propose an Eulerian-Lagrangian Runge-Kutta discontinuous Galerkin method (EL-RKDG) in [X. Cai, J.-M. Qiu, and Y. Yang, *J. Comput. Phys.*, 439 (2021), 110392], as an extension of the SL discontinuous Galerkin (DG) methods. This work is a further extension of the algorithm to unstructured triangular meshes with discussion on the treatment of inflow boundary condition. We also discuss the discrete geometric conservation law. The nonlinear WENO limiter is applied to control oscillations. Desired properties of the proposed method are numerically verified by a set of benchmarks tests.

**Key words.** Eulerian-Lagrangian; discontinuous Galerkin; unstructured triangular meshes; mass conservation; semi-Lagrangian; characteristics.

**AMS subject classifications.** 65M25, 65M60, 76M10

**1. Introduction.** The transport processes are ubiquitous in a variety of applications such as climate modeling and kinetic models. They can be described by the transport equation

$$(1.1) \quad u_t + \nabla \cdot (\mathbf{V}u) = 0,$$

where  $\mathbf{V}$  is the advection coefficient which could depend on space, time and the solution  $u$  for a nonlinear problem.

In the past decades, extensive mesh-based computational tools such as Eulerian and semi-Lagrangian (SL) approaches have been successfully developed and applied to various areas of science and engineering. For the Eulerian approach, the Runge-Kutta (RK) discontinuous Galerkin (DG) methods [16] are well-known for their properties of high resolution, compactness, flexibility for handling complex geometry, high parallel efficiency and superconvergence for long time integration, which led to successful applications to diverse application fields such as aerodynamics [57], computational geosciences [50], plasma simulation [14, 48], among many others. One drawback of the RK DG method is the stringent time stepping size with numerical stability for explicit time stepping. On the other hand, the SL approach allows extra large time stepping size by tracking solutions along characteristics. Several classes of semi-Lagrangian schemes have been developed such as the finite element based Lagrange-Galerkin

---

\*

**Funding:** Research is supported by NSF grant NSF-DMS-1818924, Air Force Office of Scientific Computing FA9550-18-1-0257 and University of Delaware.

<sup>†</sup>Advanced Institute of Natural Sciences, Beijing Normal University at Zhuhai, 519087, China, and Division of Science and Technology, United International College (BNU-HKBU), Zhuhai, 519087, China. ([xfcai@bnu.edu.cn](mailto:xfcai@bnu.edu.cn); [xiaofengcai@uic.edu.cn](mailto:xiaofengcai@uic.edu.cn)).

<sup>‡</sup>Department of Mathematical Sciences, University of Delaware, Newark, DE, 19716, USA. ([jingqiu@udel.edu](mailto:jingqiu@udel.edu)).

method (or the Characteristic-Galerkin method) [39, 20, 36] and their extensions [11, 44, 53, 46], finite difference based [40, 29], finite volume based [37, 24, 30, 34, 17], DG based [41, 43, 28, 31, 6, 5, 18], and unstructured meshes based [4, 3]. Recently, the multi-dimensional SLDG method is proposed in [8, 31] methods. For the nonlinear dynamics, the SL method can be coupled with the high order prediction-correction method [9] or the exponential integrators [7] for nonlinear characteristic tracing. For theoretical analysis, the optimal convergence and superconvergence of SLDG schemes for linear convection equations in one space dimension are shown in [54].

One significant limitation of the SL approach is to efficiently track characteristics in a nonlinear, truly multi-dimensional and highly accurate fashion. For example, in order to achieve third order spatial accuracy, sides of upstream cells have to be approximated by quadratic curves in a general setting. This introduces extra computational complexity, especially when extended to problems with dimension higher than two. In addition, to resolve the nonlinearity, some prediction-correction strategy or the exponential integrators [9, 7] have to be introduced. To address these challenges, we proposed a novel Eulerian-Lagrangian (EL) DG method in [10]. The EL DG method is a generalization of the SL DG method [8]. The SLDG method is formulated based on the design of a localized adjoint problem for the test function that exactly tracks characteristics; while in the EL DG method, the adjoint problem for the test function does not need to follow exact characteristics, but only approximately. Such feature allows flexibility, especially for high dimensional and nonlinear problems, where characteristics are difficult to track. The errors that occurred in approximating characteristics will be integrated in time by RK methods via the method-of-lines approach. Thus the fully discrete EL DG scheme will be termed EL RK DG method. Note that the SL DG in [8] and EL RK DG in [10] are based on the Cartesian meshes. With the consideration of complex geometry for practical applications, this paper extends the EL RK DG method to unstructured triangular mesh.

We propose Eulerian-Lagrangian schemes on the unstructured mesh that satisfy the following essential properties for transport problems: mass conservation, high order accuracy in both space and time, stability with extra large time-stepping sizes, and essentially non-oscillatory for discontinuities. To conserve the total mass, the exact evaluation of the integral over the upstream cell that overlaps multiple background elements is crucial but very challenging. To tackle this difficulty, we propose a remapping algorithm by local mesh intersection that is mass conservative, where the evaluation of integrals is stable and accurate via a subregion-by-subregion fashion; other conservative remapping algorithms by local mesh intersection can be found in [2, 23, 22, 1]. We first propose a second order, unconditionally stable, and mass conservative SLDG method on the triangular meshes. Then we propose a high order EL RK DG method on the triangular meshes. Note that the evolution step of EL RK DG coincides with the arbitrary Lagrangian-Eulerian (ALE) DG scheme [26], from which we extend the discussion of discrete geometric conservation law (GCL) to the proposed EL RK DG method. In addition, we have discussions on inflow boundary condition and nonlinear WENO limiters [59] to control oscillations around discontinuities. As an initial effort, we confine our attention to the linear transport equations when  $\mathbf{V}$  is independent of solution  $u$ .

The rest of this paper is arranged as follows. In Section 2.2, we propose a second order conservative SL DG method on unstructured mesh; in Section 2.3, we propose a high order EL RK DG method on the triangular meshes together with the discussion on the discrete geometric conservation laws and the treatment of inflow boundary condition in Sections 2.4-2.5 respectively. In Section 3, we provide numerical results

to showcase favorable properties of the proposed schemes. Finally, concluding remarks are made in Section 4.

## 2. SL DG and EL RK DG on unstructured meshes.

**2.1. A 2D transport problem and notations.** We consider a 2D linear transport equation in a conservative form

$$(2.1) \quad u_t + \nabla_{x,y} \cdot (\mathbf{V}(x, y, t)u) = 0,$$

with continuous velocity field  $\mathbf{V}(x, y, t) = (a(x, y, t), b(x, y, t))$  on a polygonal domain  $\Omega$ , a given initial condition and proper boundary conditions. In this paper, either the inflow/outflow or periodic boundary conditions will be considered. We generate a fixed background mesh which is a partition of  $\Omega$  by a set of triangular elements  $K_j$ ,  $j = 1, \dots, J$  and let  $h = \sup_j \text{diam}(K_j)$ , where  $\text{diam}(K_j)$  denotes the diameter of  $K_j$ . We define the finite dimensional DG approximation space as  $V_h^k = \{v_h : v_h|_{K_j} \in P^k(K_j)\}$ , in which  $P^k(K_j)$  denotes the space of polynomials in  $K_j$  of degree at most  $k$ . In particular  $P^k(K_j) = \text{Span}(\Psi_i^{K_j} : i = 1, \dots, n_k)$  with the dimension  $n_k = \frac{(k+1)(k+2)}{2}$ , where  $\Psi_i^{K_j}, i = 1, \dots, n_k$  are an orthogonal basis on  $K_j$ .

**2.2. The SL DG method.** In this section, we propose a conservative SL DG method on unstructured triangular meshes. The scheme uses linear functions to approximate sides of upstream cells. Note that the integral evaluations on the upstream cells that overlap with several background cells are important for mass conservation [36] and are performed by a new remapping algorithm, different from a direct application of numerical quadratures on the upstream cells [55]. It will be an important step for the higher-order EL RK DG algorithm introduced next.

To update the numerical solution from time level  $t^n$  to time level  $t^{n+1}$  over element  $K_j$ , we consider an adjoint problem for the test function  $\psi(x, y, t)$ :

$$(2.2) \quad \psi_t + \mathbf{V}(x, y, t) \cdot \nabla_{x,y} \psi = 0, \quad \psi(x, y, t = t^{n+1}) = \Psi(x, y) \in P^k(K_j),$$

for which the test function  $\psi$  stays constant along characteristic trajectories. As shown in [8], we have

$$\frac{d}{dt} \int_{K_j(t)} u(x, y, t) \psi(x, y, t) dx dy = 0,$$

where  $K_j(t)$  is a dynamic moving element, emanating from the Eulerian element  $K_j$  at  $t^{n+1}$  backward in time by following the characteristic trajectories. The SLDG scheme is formulated as follows: given the approximate solution  $u_h^n \in V_h^k$  at time level  $t^n$ , to find the solution  $u_h^{n+1}|_{K_j} \in V_h^k$ , such that for  $\Psi_i^{K_j} \in P^k(K_j)$ ,  $i = 1, \dots, n_k$ , we have

$$(2.3) \quad \int_{K_j} u_h^{n+1} \Psi_i^{K_j}(x, y) dx dy = \int_{K_j^*} u_h^n \Psi_i^{K_j}(x, y, t^n) dx dy,$$

where  $K_j^* := K_j(t^n)$  denotes the upstream element of the element  $K_j$  following the characteristics backward to  $t^n$ , see the deformed element bounded by blue curves in Figure 2.1 (a); and  $\Psi_i^{K_j}(x, y, t^n)$  comes from tracking along characteristics from solving the final value adjoint problem (2.2).

The SLDG method boils down to evaluate the right-hand side (R.H.S.) of (2.3), which consists of three parts: (1) the upstream element can be approximated by a

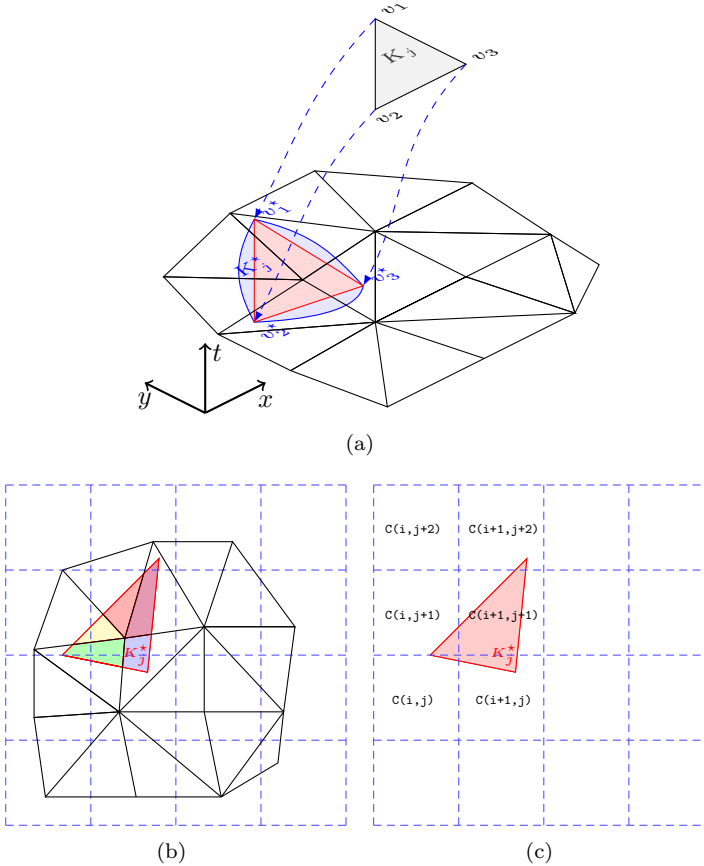


FIG. 2.1. Illustration of SLDG with triangular approximation. (c):  $K_j^*$  connects the potential boxes:  $C(i, j)$ ,  $C(i, j+1)$ ,  $C(i, j+2)$ ,  $C(i+1, j)$ ,  $C(i+1, j+1)$ ,  $C(i+1, j+2)$ .

triangle (subject to a second order accuracy), and below we still use  $K_j^*$  to represent this triangle, as shown in Figure 2.1; (2)  $\psi_i^{K_j}(x, y, t^n)$  is unknown on  $K_j^*$ , and we adopt an interpolation to reconstruct it based on the fact that the test function stays constant along characteristic trajectories; (3)  $u_h^n$  is the DG solution that is discontinuous across element interfaces of the background mesh (black lines in Figure 2.1 (b)), and thus the evaluation of (2.3) should be evaluated in a subregion-by-region manner. Accordingly, the procedure of the SLDG method is performed as follows.

**1. Characteristic tracing.** The three vertices of  $K_j$  with the coordinate  $(x_{j,q}, y_{j,q})$  are denoted by  $v_q, q = 1, 2, 3$ . We trace characteristic trajectories backward in time from time level  $t^{n+1}$  to time level  $t^n$  for  $v_q$  by using a high order RK method to solve the characteristics equations,

$$\begin{cases} \frac{dx(t)}{dt} = a(x, y, t), \\ \frac{dy(t)}{dt} = b(x, y, t), \\ x(t^{n+1}) = x_{j,q}, y(t^{n+1}) = y_{j,q}, \end{cases}$$

and obtain  $v_q^*$  with the new coordinate  $(x_{j,q}^*, y_{j,q}^*), q = 1, 2, 3$ .

2. **Interpolation for test function**  $\psi_i^{K_j}(x, y, t^n)$ . We use a polynomial interpolation to approximate the test function  $\psi_i^{K_j}(x, y, t^n)$ , based on the fact that  $\psi_i^{K_j}$  stays constant along characteristics; for instance, for  $k = 1$ , we reconstruct a  $P^1$  polynomial  $\psi_i^{K_j^*}(x, y)$  by the interpolation constraints  $\psi_i^{K_j^*}(x_{j,q}^*, y_{j,q}^*) = \Psi_i^{K_j}(x_{j,q}, y_{j,q}), q = 1, 2, 3$ .

3. **An SLDG remapping algorithm.** When  $K_j^*$  overlaps with  $K_l$  in the background mesh, one can identify overlapping subregions (denoted by  $K_{j,l}^*$  and plotted in different colors in Figure 2.1 (b)), and compute the integral (2.3) subregion-by-subregion. Subregions can be identified by an algorithm to determine the intersection regions illustrated in Figure 2.1 (b), and the subregion integrals can be done by dividing subregions into triangles as in [32] (denoted by  $K_{j,T_m}^*$ ) and applying triangular quadrature rules in the reference element as in [31]. We denote the solution and test function at quadrature point by  $u_{i_g}^{K_{j,T_m}^*}$  and  $\psi_{i,i_g}^{K_{j,T_m}^*}$ , respectively. The corresponding weight and the area of  $K_{j,T_m}^*$  are denoted by  $w_{i_g}, |K_{j,T_m}^*|$ . The formulation of this remapping algorithm is summarized as follows: for  $K_j^*$ ,

$$\begin{aligned}
& \int_{K_j^*} u_h(x, y, t^n) \psi_i^{K_j^*}(x, y) dx dy \\
&= \sum_l \int_{K_{j,l}^*} u_h(x, y, t^n) \psi_i^{K_j^*}(x, y) dx dy \\
&= \sum_m \int_{K_{j,T_m}^*} u_h(x, y, t^n) \psi_i^{K_j^*}(x, y) dx dy \\
(2.4) \quad &= \sum_m \sum_{i_g} u_{i_g}^{K_{j,T_m}^*} \psi_{i,i_g}^{K_{j,T_m}^*} w_{i_g} |K_{j,T_m}^*| := \tilde{U}_i^{K_j}(t^n).
\end{aligned}$$

The key step of the remapping algorithm is to search  $K_{j,l}^*$  which is the overlapping subregion by the upstream element  $K_j^*$  and the Eulerian element  $K_l$ . Then we summarize the SLDG remapping algorithm as follows:

**Step 1.** To search the elements  $K_l$  that intersect with the upstream element  $K_j^*$ , we generate an auxiliary rectangular mesh to create a location look-up table, with which we provide a look-up table for the location of  $K_l$ , as indicated in Figure 2.1 (c).

**Step 2.** Perform the Sutherland-Hodgman clipping algorithm in [47, 13] for  $K_j^*$  and  $K_l$  to get  $K_{j,l}^*$  and cut it into a set of sub-triangles  $K_{j,T_m}^*$ .

**Step 3.** The final  $L^2$  projection (2.4) can be done since given  $K_{j,T_m}^*$ 's vertices and location in the background mesh, we can have  $|K_{j,T_m}^*|$ , quadrature points and corresponding  $u_{i_g}^{K_{j,T_m}^*}, \psi_{i,i_g}^{K_{j,T_m}^*}$  in this sub-triangle.

**PROPOSITION 2.1.** *Given a DG solution  $u_h(x, y, t^n) \in V_h^k$  and assuming the boundary condition is periodic, the proposed SLDG scheme on the unstructured mesh (2.3) is mass conservative. In particular,*

$$(2.5) \quad \sum_{j=1}^J \int_{K_j} u_h(x, y, t^{n+1}) dx dy = \sum_{j=1}^J \int_{K_j} u_h(x, y, t^n) dx dy.$$

*Proof.* The proof can be done by letting  $\Psi(x, y) = 1$  and recombining  $K_{j,l}^*$  to the background mesh  $K_j$  as well as using the periodically boundary condition as that of SLDG on the structured mesh in [8].  $\square$

**2.3. The EL-RKDG method.** In this section, we propose a general high-order EL-RKDG method on the unstructured triangular meshes, which is a generalization of the SLDG method [28, 8] and the RKDG method [16]. The proposed EL-RKDG method of exactly mass conservative and largely alleviates the CFL condition of the RKDG method.

We start to formulate the EL-RKDG scheme by a modified adjoint problem on the associated space-time region. The formulation can be viewed as a composition of the ALE scheme [26] and the SLDG remapping algorithm in the previous section.

**(1) A modified adjoint problem for the 2D transport equation.** Consider a *modified* adjoint problem:

$$(2.6) \quad \psi_t + \tilde{\mathbf{V}}(x, y, t) \cdot \nabla_{x,y} \psi = 0, \quad \psi(x, y, t = t^{n+1}) = \Psi(x, y) \in P^k(K_j),$$

where  $\tilde{\mathbf{V}}(x, y, t) = (\alpha(x, y, t), \beta(x, y, t))$  are defined as follows:

1. **On  $K_j$  at  $t^{n+1}$ .**  $\alpha(x, y, t^{n+1})$  and  $\beta(x, y, t^{n+1})$  are set as  $P^1$  polynomials denoted by

$$(2.7) \quad \alpha(x, y, t^{n+1}) = \alpha_0 + \alpha_1 x + \alpha_2 y,$$

$$(2.8) \quad \beta(x, y, t^{n+1}) = \beta_0 + \beta_1 x + \beta_2 y.$$

As in [10],  $\alpha$  and  $\beta$  are linear functions interpolating  $\mathbf{V}(x, y, t)$  at vertices of  $K_j$  at the time level  $t^{n+1}$ .

2. **On  $\tilde{K}_j(t)$  at  $t \in [t^n, t^{n+1}]$ .** Along characteristic lines of the adjoint problem (2.6) originating from any point  $(X, Y) \in K_j$  at  $t^{n+1}$ , with

$$(2.9) \quad \tilde{x}(t; (X, Y, t^{n+1})), \tilde{y}(t; (X, Y, t^{n+1}))$$

satisfying the following equations,

$$(2.10) \quad \frac{d}{dt} \tilde{x}(t; (X, Y, t^{n+1})) = \alpha(X, Y, t^{n+1}), \quad \frac{d}{dt} \tilde{y}(t; (X, Y, t^{n+1})) = \beta(X, Y, t^{n+1}).$$

Note that the right-hand side of above equations are independent of  $t$ , then solving these equations that originate from  $(X, Y)$ , we have

$$(2.11) \quad \tilde{x}(t; (X, Y, t^{n+1})) = X - \alpha(X, Y, t^{n+1})(t^{n+1} - t),$$

$$(2.12) \quad \tilde{y}(t; (X, Y, t^{n+1})) = Y - \beta(X, Y, t^{n+1})(t^{n+1} - t).$$

The associated space-time region for (2.6) then becomes  $\tilde{\Omega}_j := \tilde{K}_j(t) \times [t^n, t^{n+1}]$ , where  $\tilde{K}_j(t)$  is the triangle with vertices along straight characteristic lines originated from vertices of  $K_j$ , see Figure 2.2 (a).

Then, for  $(\tilde{x}(t), \tilde{y}(t)) := (\tilde{x}(t; (X, Y, t^{n+1})), \tilde{y}(t; (X, Y, t^{n+1}))) \in \tilde{K}_j(t)$ , where  $t \in [t^n, t^{n+1}]$ , the  $\tilde{\mathbf{V}}(x, y, t)$  is defined as

$$(2.13) \quad \begin{aligned} \tilde{\mathbf{V}}(\tilde{x}(t), \tilde{y}(t), t) &= \begin{pmatrix} \alpha(\tilde{x}(t; (X, Y, t^{n+1})), \tilde{y}(t; (X, Y, t^{n+1})), t) \\ \beta(\tilde{x}(t; (X, Y, t^{n+1})), \tilde{y}(t; (X, Y, t^{n+1})), t) \end{pmatrix} \\ &= \begin{pmatrix} \alpha(X, Y, t^{n+1}) \\ \beta(X, Y, t^{n+1}) \end{pmatrix}. \end{aligned}$$

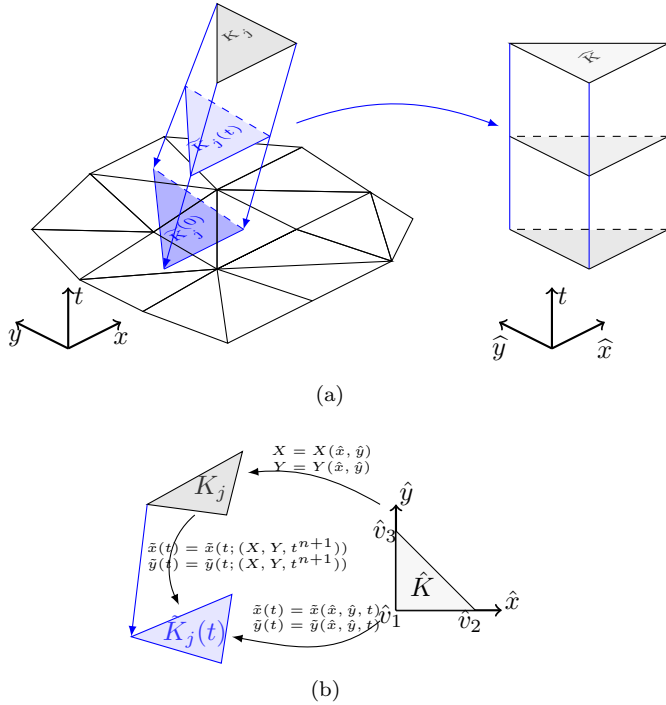


FIG. 2.2. (a): illustration of the space-time region  $\tilde{K}_j(t) \times [t^n, t^{n+1}]$ ; (b): the mapping between dynamic element  $\tilde{K}_j(t)$  and the reference element  $\hat{K}$ .

We summarize several properties of the modified adjoint problem in the following proposition.

PROPOSITION 2.2. *For the modified adjoint problem, we have*

(i) *its characteristic lines,*

$$(2.14) \quad \tilde{x}(t; (X, Y, t^{n+1})), \tilde{y}(t; (X, Y, t^{n+1})),$$

*for any point  $(X, Y) \in K_j$  at  $t^{n+1}$ , can be explicitly presented as*

$$(2.15) \quad \begin{pmatrix} \tilde{x}(t) \\ \tilde{y}(t) \end{pmatrix} = \mathbf{J}^{\tilde{K}_j K_j}(t) \begin{pmatrix} X \\ Y \end{pmatrix} + \begin{pmatrix} \delta_1(t) \\ \delta_2(t) \end{pmatrix},$$

*with the merely time-dependent Jacobian matrix denoted by*

$$(2.16) \quad \mathbf{J}^{\tilde{K}_j K_j}(t) := \frac{\partial(\tilde{x}, \tilde{y})}{\partial(X, Y)}(t) := \begin{pmatrix} 1 - \frac{\partial\alpha}{\partial X}(t^{n+1} - t) & -\frac{\partial\alpha}{\partial Y}(t^{n+1} - t) \\ -\frac{\partial\beta}{\partial X}(t^{n+1} - t) & 1 - \frac{\partial\beta}{\partial Y}(t^{n+1} - t) \end{pmatrix},$$

*where  $\delta_1(t) := (t - t^{n+1})\alpha_0$ ,  $\delta_2(t) := (t - t^{n+1})\beta_0$ .*

(ii)

$$(2.17) \quad \psi(\tilde{x}(t; (x, y, t^{n+1})), \tilde{y}(t; (x, y, t^{n+1})), t) = \Psi(x, y) \in P^k(K_j), \quad \forall t \in [t^n, t^{n+1}].$$

*Proof.* Firstly, the equation (2.15) can be easily obtained by substituting (2.7) and (2.8) into (2.11) and (2.12).

Secondly, we can prove (2.17) by the fact that the test function  $\psi$  stays constant along characteristics.  $\square$

**(2) Semi-discrete EL-RKDG formulation.** Integrate (2.1)  $\cdot \psi +$  (2.6)  $\cdot u$  over  $\tilde{\Omega}_j$ , that is,

$$(2.18) \quad \int_{\tilde{\Omega}_j} [(\text{2.1}) \cdot \psi + (\text{2.6}) \cdot u] dx dy dt = 0.$$

After manipulating the above equation with the divergence theorem and the Leibniz-Reynolds transport theorem and considering its time differential form, we have

$$(2.19) \quad \frac{d}{dt} \int_{\tilde{K}_j(t)} u \psi dx dy = - \int_{\partial \tilde{K}_j(t)} \psi \mathbf{F} \cdot \mathbf{n} ds + \int_{\tilde{K}_j(t)} \mathbf{F} \cdot \nabla \psi dx dy,$$

where  $\mathbf{F}(u, x, y, t) = (\mathbf{V}(x, y, t) - \tilde{\mathbf{V}}(x, y, t)) u$ ,  $ds$  is the infinitesimal boundary of  $\tilde{K}_j(t)$ , and  $\mathbf{n}$  denotes the unit outward normal vector to  $\partial \tilde{K}_j(t)$ .

To facilitate implementation, we map the semi-discrete EL-RKDG formulation on the reference element  $\hat{K}$  with vertices  $\hat{v}_1(0, 0)$ ,  $\hat{v}_2(1, 0)$ , and  $\hat{v}_3(0, 1)$  (see Figure 2.2 (b)). We denote the isoparametric mapping functions from the reference element  $\hat{K}$  to the Eulerian element  $K_j$  and the dynamic element  $\tilde{K}_j(t)$  by  $(X(\hat{x}, \hat{y}), Y(\hat{x}, \hat{y}))^T$  and  $(\tilde{x}(\hat{x}, \hat{y}, t), \tilde{y}(\hat{x}, \hat{y}, t))^T$ , respectively. We can easily have

$$(2.20) \quad \begin{pmatrix} X(\hat{x}, \hat{y}) \\ Y(\hat{x}, \hat{y}) \end{pmatrix} = \mathbf{J}^{K_j \hat{K}_j} \begin{pmatrix} \hat{x} \\ \hat{y} \end{pmatrix} + \begin{pmatrix} x_{j,1} \\ y_{j,1} \end{pmatrix},$$

where

$$(2.21) \quad \mathbf{J}^{K_j \hat{K}_j} = \begin{pmatrix} x_{j,2} - x_{j,1} & x_{j,3} - x_{j,1} \\ y_{j,2} - y_{j,1} & y_{j,3} - y_{j,1} \end{pmatrix}.$$

Then the mapping function  $(\tilde{x}(\hat{x}, \hat{y}, t), \tilde{y}(\hat{x}, \hat{y}, t))^T$  can be presented as:

$$(2.22) \quad \begin{pmatrix} \tilde{x}(\hat{x}, \hat{y}, t) \\ \tilde{y}(\hat{x}, \hat{y}, t) \end{pmatrix} = \mathbf{J}^{\tilde{K}_j \hat{K}_j(t)} \begin{pmatrix} \hat{x} \\ \hat{y} \end{pmatrix} + \mathbf{J}^{\tilde{K}_j \hat{K}_j(t)} \begin{pmatrix} x_{j,1} \\ y_{j,1} \end{pmatrix} + \begin{pmatrix} \delta_1(t) \\ \delta_2(t) \end{pmatrix},$$

where  $\mathbf{J}^{\tilde{K}_j \hat{K}_j(t)} = \mathbf{J}^{\tilde{K}_j K_j(t)} \mathbf{J}^{K_j \hat{K}_j}$ , that is, the Jacobian of the mapping functions with respect to variables  $\hat{x}, \hat{y}$ .

Next we introduce a few notations and useful equalities [15, 38] regarding this mapping function.

$$(2.23) \quad d\tilde{x} d\tilde{y} = \det \left( \mathbf{J}^{\tilde{K}_j \hat{K}_j(t)} \right) d\hat{x} d\hat{y},$$

$$(2.24) \quad \nabla_{\tilde{x}, \tilde{y}} \psi(\tilde{x}, \tilde{y}, t) = \mathbf{J}^{\tilde{K}_j \hat{K}_j(t)} \mathbf{J}^{K_j \hat{K}_j(t)} \nabla_{\hat{x}, \hat{y}} \Psi(\hat{x}, \hat{y}),$$

$$(2.25) \quad \mathbf{n} ds = \det \left( \mathbf{J}^{\tilde{K}_j \hat{K}_j(t)} \right) \mathbf{J}^{\tilde{K}_j \hat{K}_j(t)} \mathbf{J}^{K_j \hat{K}_j(t)} \mathbf{n} d\hat{s},$$

where  $d\check{s}$  is the infinitesimal boundary of the isoparametric element and  $\check{\mathbf{n}}$  denotes the unit outward normal vector to  $\partial\hat{K}$ .

We denote the approximation solution of  $u$  on the reference element by  
(2.26)

$$\hat{u}_h(\hat{x}, \hat{y}, t) := \sum_{j=1}^J \sum_{p=1}^{n_k} \check{u}_p^{K_j}(t) \hat{\Psi}_p^{K_j}(\hat{x}, \hat{y}) := \sum_{p=1}^{Jn_k} \check{u}_p(t) \hat{\Psi}_p(\hat{x}, \hat{y}), \text{ for all } t \in [t^n, t^{n+1}],$$

where  $\hat{\Psi}_p^{K_j}(\hat{x}, \hat{y})$  denotes  $\Psi_p^{K_j}(X(\hat{x}, \hat{y}), Y(\hat{x}, \hat{y}))$ , we rename  $\{\check{u}_p^{K_j}(t) : 1 \leq p \leq n_k, 1 \leq j \leq J\} = \{\check{u}_p(t) : 1 \leq p \leq Jn_k\}$  and  $\{\hat{\Psi}_p^{K_j} : 1 \leq p \leq n_k, 1 \leq j \leq J\} = \{\hat{\Psi}_p : 1 \leq p \leq Jn_k\}$ . We rewrite the semi-discrete EL-RKDG formulation (2.19) on the reference element  $\hat{K}$  as follows:  $\forall \Psi_q(X, Y) \in V_h^k$ ,

$$(2.27) \quad \begin{aligned} & \frac{d}{dt} \int_{\hat{K}} \hat{u}_h \hat{\Psi}_q \det \left( \mathbf{J}^{\tilde{K}_j \hat{K}_j}(t) \right) d\hat{x} d\hat{y} \\ &= - \int_{\partial\hat{K}} \hat{\Psi}_q \hat{F} d\check{s} + \int_{\hat{K}} \hat{\mathbf{F}} \cdot \left( \mathbf{J}^{\tilde{K}_j \hat{K}_j}(t)^{-T} \nabla_{\hat{x}, \hat{y}} \hat{\Psi}_q \right) \det \left( \mathbf{J}^{\tilde{K}_j \hat{K}_j}(t) \right) d\hat{x} d\hat{y}, \end{aligned}$$

where

$$(2.28) \quad \hat{\mathbf{F}}(\hat{u}_h, \hat{x}, \hat{y}, t) := \bar{\mathbf{V}} \hat{u}_h,$$

with

$$(2.29) \quad \bar{\mathbf{V}} := \left( \mathbf{V}(\tilde{x}(\hat{x}, \hat{y}, t), \tilde{y}(\hat{x}, \hat{y}, t), t) - \tilde{\mathbf{V}}(X(\hat{x}, \hat{y}), Y(\hat{x}, \hat{y}), t^{n+1}) \right),$$

and we define the upwind numerical flux as

$$(2.30) \quad \hat{F} \left( \hat{u}_h^{int_{\hat{K}}}, \hat{u}_h^{ext_{\hat{K}}}, \hat{x}, \hat{y}, t, \mathbf{J}^{\tilde{K}_j \hat{K}_j}(t) \right) = W u^{\text{up}}$$

with

$$(2.31) \quad W = \bar{\mathbf{V}} \cdot \left( \det \left( \mathbf{J}^{\tilde{K}_j \hat{K}_j}(t) \right) \mathbf{J}^{\tilde{K}_j \hat{K}_j}(t)^{-T} \check{\mathbf{n}} \right)$$

and

$$(2.32) \quad u^{\text{up}} = \begin{cases} \hat{u}_h^{int_{\hat{K}}} & \text{if } W \geq 0, \\ \hat{u}_h^{ext_{\hat{K}}} & \text{if } W < 0. \end{cases}$$

Here  $\hat{u}_h^{int_{\hat{K}}}$  and  $\hat{u}_h^{ext_{\hat{K}}}$  are the interior solution and the exterior solution of the  $\tilde{K}_j(t)$ , respectively. The line and volume integrals are performed by proper high order quadrature rules [21, 42] which are exact for polynomials of degree up to  $2k$  for the element integral and up to  $2k+1$  for the edge integral as in a standard RKDG scheme. Then we have

$$(2.33) \quad \frac{d}{dt} \int_{\hat{K}} \hat{u}_h \hat{\Psi}_q \det \left( \mathbf{J}^{\tilde{K}_j \hat{K}_j}(t) \right) d\hat{x} d\hat{y} = \mathcal{G} \left( \hat{u}_h, \mathbf{J}^{\tilde{K}_j \hat{K}_j}(t) \right),$$

where

$$(2.34) \quad \begin{aligned} & \mathcal{G} \left( \hat{u}_h, \mathbf{J}^{\tilde{K}_j \hat{K}_j}(t) \right) := - \sum_{e \in \partial\hat{K}} |e| \sum_{i_e} \left[ \hat{\Psi}_q \hat{F} \right] \Big|_{(\hat{x}_{i_e}, \hat{y}_{i_e})} \sigma_{i_e} \\ & + 2|\hat{K}| \sum_i \left[ \hat{\mathbf{F}} \cdot \left( \mathbf{J}^{\tilde{K}_j \hat{K}_j}(t)^{-T} \nabla_{\hat{x}, \hat{y}} \hat{\Psi}_q \right) \det \left( \mathbf{J}^{\tilde{K}_j \hat{K}_j}(t) \right) \right] \Big|_{(\hat{x}_i, \hat{y}_i)} w_i, \end{aligned}$$

with the numerical quadrature points  $(\hat{x}_{i_e}, \hat{y}_{i_e})$  and corresponding weights  $\sigma_{i_e}$  for the edge integral, and the numerical quadrature points  $(\hat{x}_i, \hat{y}_i)$  and corresponding weights  $w_i$  for the element integral.

**(3) Fully-discrete EL-RKDG scheme.** We write the semi-discrete scheme (2.33) into a form of ordinary differential equations with the initial conditions. We let  $\check{\mathbf{u}}(t)$  be a vector in  $\mathbb{R}^{Jn_k}$  which consists of unknowns  $\{\check{u}_p(t) : 1 \leq p \leq Jn_k\}$ , and denote the spatial discretization operator of the R.H.S. of (2.33) by  $\mathcal{L}(\check{\mathbf{u}}(t), t)$ . Then the semi-discrete scheme (2.33) can be written as

$$(2.35) \quad \frac{d}{dt} (\mathbf{M}(t)\check{\mathbf{u}}(t)) = \mathcal{L}(\check{\mathbf{u}}(t), t), \quad \check{\mathbf{u}}(t^n) = \check{\mathbf{u}}^n,$$

where the matrix  $\mathbf{M}(t) = (M_{pq}(t))_{pq}$  with block diagonals,

$$\text{diag}(\mathbf{M}^{K_1}(t), \dots, \mathbf{M}^{K_J}(t));$$

for  $\mathbf{M}^{K_j}(t)$ , its element

$$(2.36) \quad \begin{aligned} M_{pq}^{K_j}(t) &= \int_{\tilde{K}} \hat{\Psi}_p^{K_j}(\hat{x}, \hat{y}) \hat{\Psi}_q^{K_j}(\hat{x}, \hat{y}) \det(\mathbf{J}^{\tilde{K}_j K_j}(t)) d\hat{x} d\hat{y} \\ &= \int_{\tilde{K}_j(t)} \psi_p^{K_j}(x, y, t) \psi_q^{K_j}(x, y, t) dx dy \\ &= \int_{K_j} \Psi_p^{K_j}(X, Y) \Psi_q^{K_j}(X, Y) \det(\mathbf{J}^{\tilde{K}_j K_j}(t)) dX dY \\ &= \det(\mathbf{J}^{\tilde{K}_j K_j}(t)) \int_{K_j} \Psi_p^{K_j}(X, Y) \Psi_q^{K_j}(X, Y) dX dY, \end{aligned}$$

where the last equality is due to the space-independency of  $\det(\mathbf{J}^{\tilde{K}_j K_j}(t))$ . The following steps are proposed for updating the system (2.35).

1. **Building the space-time region.** In order to update the system (2.35) by the ALE scheme, we build the space-time region  $\tilde{\Omega}$  and pre-compute the Jacobians at immediate stages of the Runge-Kutta method; the coordinates of vertices of the upstream element can be easily obtained from (2.11)-(2.12).
2. **The test function  $\psi_p^{K_j}(x, y, t^n)$ .** The test function  $\psi_p^{K_j}(x, y, t^n)$  can be provided explicitly due to the local affine mapping (2.15).
3. **Remapping step.** We apply the remapping algorithm as proposed for the SLDG in Section 2.2 to compute

$$(2.37) \quad \int_{K_j^*} u_h^n \psi_p^{K_j}(x, y, t^n) dx dy := \tilde{U}_p^{K_j}(t^n).$$

We rename  $\{\tilde{U}_p^{K_j}(t) : 1 \leq p \leq n_k, 1 \leq j \leq J\} := \{\tilde{U}_p(t) : 1 \leq p \leq Jn_k\}$ , all elements of which form the vector  $\tilde{\mathbf{U}}(t)$ . Then the initial condition in (2.35) can be obtained as

$$(2.38) \quad \check{\mathbf{u}}^n = \mathbf{M}(t^n)^{-1} \tilde{\mathbf{U}}(t^n), \quad p = 1 \dots Jn_k,$$

where  $\mathbf{M}(t^n)$  comes from (2.36) and  $\tilde{\mathbf{U}}(t^n)$  comes from (2.37) via the remapping algorithm.

---

**Algorithm 2.1** The  $s$ -stages SSP-RK time discretization for the system (2.35).

---

Let  $\check{\mathbf{u}}^{(0)} = \check{\mathbf{u}}^n$ ; For RK stage  $i = 1, \dots, s$ ,

$$(2.39) \quad \check{\mathbf{u}}^{(i)} = \mathbf{M}(t^n + d_i \Delta t^n)^{-1} \sum_{l=0}^{i-1} \left( \alpha_{il} \mathbf{M}(t + d_l \Delta t^n) \check{\mathbf{u}}^{(l)} + \beta_{il} \Delta t^n \mathcal{L} \left( \check{\mathbf{u}}^{(l)}, t^n + d_l \Delta t^n \right) \right),$$

where  $\Delta t^n = t^{n+1} - t^n$ , and  $\alpha_{il}$  and  $\beta_{il}$  are related to the RK method;

$$(2.40) \quad \check{\mathbf{u}}^{n+1} = \check{\mathbf{u}}^{(s)}.$$


---

TABLE 2.1  
Parameters of SSP-RK2 and SSP-RK3.

Order	$\alpha_{il}$	$\beta_{il}$	$d_l$
2	1	1	0
	$\frac{1}{2}$	$\frac{1}{2}$	$\frac{1}{2}$
3	1	1	0
	$\frac{3}{4}$	$\frac{1}{4}$	$\frac{1}{4}$
	$\frac{1}{3}$	$0$	$\frac{2}{3}$
	$0$	$\frac{2}{3}$	$0$
	$0$	$\frac{2}{3}$	$\frac{1}{2}$

4. **Evolution step.** We apply the strong stability preserving (SSP) RK method [45] to (2.35), which is organized in Algorithm 2.1. The parameters of the second order SSP-RK method (SSP-RK2) and the third order SSP-RK method (SSP-RK3) are provided in Table 2.1.

**PROPOSITION 2.3.** *Given a DG solution  $u_h(x, y, t^n) \in V_h^k$  and assuming the boundary condition is periodic, the fully discrete EL-RKDG scheme with SSP RK time discretization on the unstructured mesh is mass conservative.*

*Proof.* The conclusion is due to the mass conservative of the SLDG remapping algorithm and the local conservative form of integrating flux function with the unique flux at the element boundaries. We skip details for brevity.  $\square$

*Remark 2.4.* (Comparison to the ALE DG method [26]) We note that when we put the background element  $K_j$  at  $t^{n+1}$  and its upstream element  $K_j^*$  at  $t^n$  in a moving mesh setting, the formulation of EL-RKDG scheme (2.19) is the same as the ALE DG method [26] and the quasi-Lagrangian moving mesh discontinuous Galerkin method [35]. In fact, the EL-RKDG method for the problem (2.35) is the composition of SLDG remapping algorithm in evaluating  $\check{\mathbf{u}}(t^n)$  and the ALE DG method in updating solutions from  $\check{\mathbf{u}}(t^n)$  to  $\check{\mathbf{u}}(t^{n+1})$ .

*Remark 2.5.* (Empirical time step constraint for stability) Note that the time step constraint for the RKDG scheme on triangular meshes are numerically verified in [16, 12] as around

$$(2.41) \quad \Delta t \sim \frac{\min_j R_j}{\max_j \max_{\text{face}} |\mathbf{V} \cdot \mathbf{n}|}.$$

We observe that the EL-RKDG formulation has a similar spirit to applying the RKDG method with the flux term  $(\mathbf{V} - \tilde{\mathbf{V}})u$ , thus an empirical time step stability constraint

of the EL-RKDG method is

$$(2.42) \quad \Delta t \sim \frac{\min_j R_j}{\max_j \max_{\text{face}} |(\mathbf{V} - \tilde{\mathbf{V}}) \cdot \mathbf{n}|}.$$

For a smooth velocity field  $\mathbf{V}$ , by Taylor expansions, we have  $|(\mathbf{V} - \tilde{\mathbf{V}}) \cdot \mathbf{n}| = O(\Delta t) + O(h^2)$ . Combining the estimate with (2.42) gives the time step constraint for the stability of the EL-RKDG scheme on the unstructured triangular mesh,

$$(2.43) \quad \Delta t \sim \sqrt{h}.$$

This is verified in Example 3.3 with mesh refinement, that is, we refine the mesh by increasing the number of elements by a factor of around 4 and then the Maximum CFL with numerical stability could increase by a factor of around  $\sqrt{2}$ . A rigorous analysis is subject to further investigation.

**2.4. Geometric Conservation Law.** Although the EL-RKDG scheme is a fixed mesh method, we notice that an ALE scheme is embedded in the EL-RKDG scheme (2.35). Hence, the Geometric Conservation Law introduced in [51, 49, 25], i.e., the preservation of constant solutions, should be considered; that is, by letting  $\hat{u}_h$  and  $\hat{\Psi}_q$  be a constant, the obtained formulation in the following should be updated by numerical schemes exactly.

**PROPOSITION 2.6.** *Letting  $\hat{u}_h = \hat{\Psi}_q = c$  and assuming the divergence free property of  $\mathbf{V}$  (i.e.,  $\nabla_{\hat{x}, \hat{y}} \cdot \mathbf{V} = 0$ ), the semi-discrete EL-RKDG formulation on the reference element  $\hat{K}$  (2.27) can be written as follows:*

$$(2.44) \quad \frac{d}{dt} \det \left( \mathbf{J}^{\hat{K}_j \hat{K}_j}(t) \right) = \left( \nabla_{\hat{x}, \hat{y}} \cdot \left( \mathbf{J}^{\hat{K} \hat{K}}(t)^{-1} \tilde{\mathbf{V}}(X(\hat{x}, \hat{y}), Y(\hat{x}, \hat{y}), t^{n+1}) \right) \right) \det \left( \mathbf{J}^{\hat{K}_j \hat{K}_j}(t) \right).$$

*Proof.* It can be proven by substituting  $\hat{u}_h = \hat{\Psi}_q = c$  into (2.27) and then using  $\nabla_{\hat{x}, \hat{y}} \cdot \mathbf{V} = 0$ , the linear property of  $\tilde{\mathbf{V}}$  and the integration by parts.  $\square$

Note that the scheme (2.35) by the SSP RK method fails to preserve the constant solution since the Jacobian determinant  $\det \left( \mathbf{J}^{\hat{K}_j \hat{K}_j}(t) \right)$  is involved in both sides of (2.44) and is evolved approximately due to the temporal integration.

To preserve the constant solution, we need to consider the time discretization of the evolution of the Jacobian determinant (2.44) as well; we adopt the GCL correction strategy by updating the Jacobian determinant by the SSP-RK method synchronously, which was introduced in [38, 26, 56]. For implementation, we replace the system (2.35) by

$$(2.45) \quad \frac{d}{dt} \left( \tilde{\mathbf{M}}(t) \tilde{\mathbf{u}}(t) \right) = \mathcal{L}(\tilde{\mathbf{u}}(t), t), \quad \tilde{\mathbf{u}}(t^n) = \tilde{\mathbf{u}}^n,$$

$$(2.46) \quad \frac{d}{dt} \mathcal{J}_j(t) = \left( \nabla_{\hat{x}, \hat{y}} \cdot \left( \mathbf{J}^{\hat{K} \hat{K}}(t)^{-1} \tilde{\mathbf{V}}(X(\hat{x}, \hat{y}), Y(\hat{x}, \hat{y}), t^{n+1}) \right) \right) \det \left( \mathbf{J}^{\hat{K}_j \hat{K}_j}(t) \right) := \mathcal{R}(t),$$

where  $\mathcal{J}_j(t)$  is an approximation to  $\det \left( \mathbf{J}^{\hat{K}_j \hat{K}_j}(t) \right)$ ,  $\mathcal{J}_j(t^n) = \det \left( \mathbf{J}^{\hat{K} \hat{K}}(t^n) \right)$ , and the matrix  $\tilde{\mathbf{M}}(t) = \left( \tilde{M}_{pq}(t) \right)_{pq}$  with block diagonals  $\text{diag} \left( \tilde{\mathbf{M}}^{K_1}(t), \dots, \tilde{\mathbf{M}}^{K_J}(t) \right)$ . The

element of  $\widetilde{\mathbf{M}}^{K_j}(t)$  is set as,

$$(2.47) \quad \widetilde{M}_{pq}^{K_j}(t) = M_{pq}^{K_j}(t) \frac{\mathcal{J}_j(t)}{\det(\mathbf{J}^{\tilde{K}_j \tilde{K}_j}(t))}.$$

Then we apply the  $s$ -stages SSP-RK method to the system to replace the evolution step in the EL-RKDG method, which is organized in Algorithm 2.2.

---

**Algorithm 2.2** The  $s$ -stages SSP-RK time discretization for the system (2.45)-(2.46).

---

Let  $\mathcal{J}_j^{(0)} = \mathcal{J}_j(t^n)$ ;

$$(2.48) \quad \int_{\tilde{K}} \hat{u}_h^{(0)} \hat{\Psi}_q \mathcal{J}_j^{(0)} d\hat{x} d\hat{y} = \int_{\tilde{K}} \hat{u}_h^n \hat{\Psi}_q \mathcal{J}_j(t^n) d\hat{x} d\hat{y};$$

For RK stage  $i = 1, \dots, s$ ,

$$(2.49) \quad \mathcal{J}_j^{(i)} = \sum_{l=0}^{i-1} \left( \alpha_{il} \mathcal{J}_j^{(l)} + \beta_{il} \Delta t^n \mathcal{R}(t^n + d_l \Delta t^n) \right);$$

$$(2.50) \quad \begin{aligned} & \int_{\tilde{K}} \hat{u}_h^{(i)} \hat{\Psi}_q \mathcal{J}_j^{(i)} d\hat{x} d\hat{y} \\ &= \sum_{l=0}^{i-1} \left( \alpha_{il} \int_{\tilde{K}} \hat{u}_h^{(l)} \hat{\Psi}_q \mathcal{J}_j^{(l)} d\hat{x} d\hat{y} + \beta_{il} \Delta t^n \mathcal{G} \left( \hat{u}_h^{(l)}, \mathbf{J}^{\tilde{K}_j \tilde{K}_j}(t^n + d_l \Delta t^n) \right) \right); \end{aligned}$$

$$(2.51) \quad \int_{\tilde{K}} \hat{u}_h^{n+1} \hat{\Psi}_q \det \left( \mathbf{J}^{\tilde{K}_j \tilde{K}_j}(t^{n+1}) \right) d\hat{x} d\hat{y} = \int_{\tilde{K}} \hat{u}_h^{(s)} \hat{\Psi}_q \mathcal{J}_j^{(s)} d\hat{x} d\hat{y}.$$


---

Finally, we state that the EL-RKDG scheme with (2.37)-(2.38) and the evolution step of Algorithm 2.2 satisfies the GCL when the R.H.S. of (2.27) (for instance, the problem with the velocity field being merely time-dependent, i.e.,  $\mathbf{V}(t) = (\bar{a}(t), \bar{b}(t))$ ) can be solved exactly by the numerical quadratures, which is summarized in the following proposition.

**PROPOSITION 2.7.** *(Discrete Geometric Conservation Law.) Suppose that the R.H.S. of (2.27) can be solved exactly by the numerical quadratures, an  $s$ -stage SSP-RK method with order greater than or equal to 2, and the solution at time level  $t^n$ ,  $u_h^n = c$  for all  $(x, y) \in \Omega$ . Then the solution at time level  $t^{n+1}$  of the EL-RKDG scheme with (2.37)-(2.38) and the evolution step of Algorithm 2.2,  $u_h^{n+1} = c$  for all  $(x, y) \in \Omega$ .*

*Proof.* As in Remark 2.4, the EL-RKDG method for the problem (2.35) is the composition of the SLDG remapping algorithm in evaluating  $\hat{\mathbf{u}}(t^n)$  and the ALE DG method. For the SLDG remapping algorithm, it is easy to see that when  $u_h^n = c$  for all  $(x, y) \in \Omega$ , through the remapping algorithm (2.37) and mapping solution to the reference element (2.38), we have  $\hat{u} = c$ . Then similar to the proof of GCL property of ALE DG in [26], we can show that  $u_h^{n+1} = c$  and thus omit the details.  $\square$

**2.5. Inflow boundaries.** In this section, we consider the inflow Dirichlet boundary conditions, which are often posed in applications such as subsurface contaminant transport and remediation [52]. For inflow boundary condition, we propose a ghost-cell strategy.

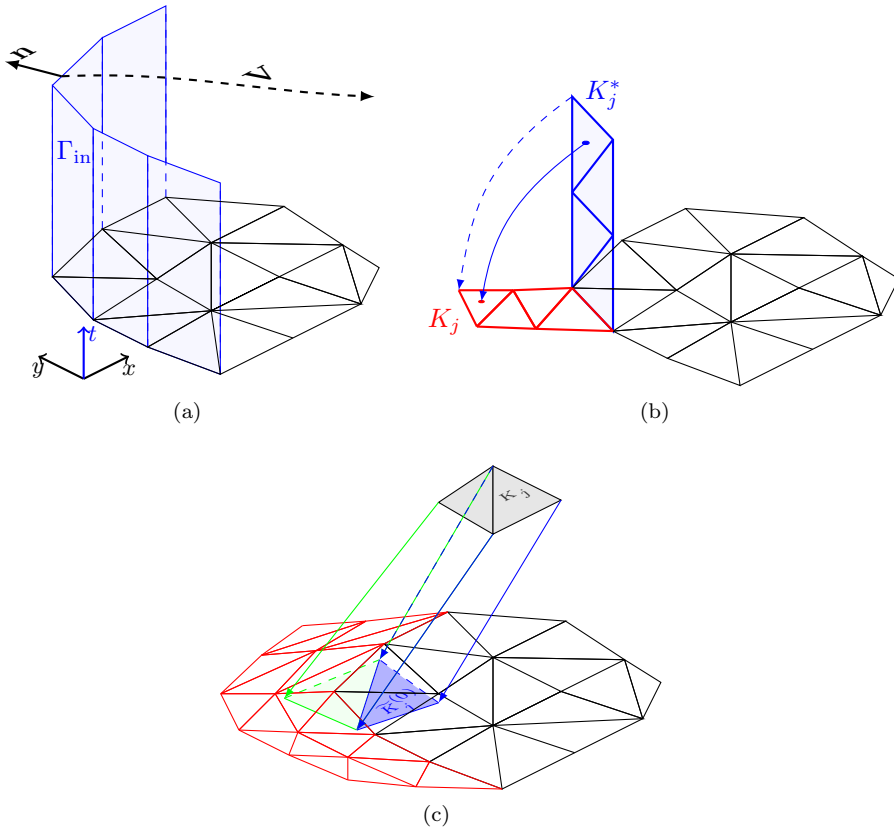


FIG. 2.3. The illustration of the EL-RKDG scheme the ghost-cells method for transport problems with inflow boundary conditions.

Let  $\partial\Omega$  be the boundary of  $\Omega$ , and  $\Gamma := \partial\Omega \times (0, T)$ , consisting of two parts: the inflow part  $\Gamma_{\text{in}}$  and outflow part  $\Gamma_{\text{out}}$  with

$$\Gamma_{\text{in}} := \{(x, y, t) | (x, y) \in \partial\Omega, t \in (0, T), \mathbf{V} \cdot \mathbf{n} < 0\}, \quad \Gamma_{\text{out}} = \Gamma \setminus \Gamma_{\text{in}}.$$

We consider the transport problem (2.1) with the inflow Dirichlet boundary condition

$$u(x, y, t) = g(x, y, t), \quad (x, y, t) \in \Gamma_{\text{in}}.$$

The scheme proceeds on a large enough ghost region by first building DG solutions on ghost cells by a Lagrangian procedure. Once it is done, the EL-RKDG scheme in Section 2.3 can be implemented, as illustrated in Figure 2.3 (c). The procedure of building DG solutions on ghost cells consists of several steps:

1. Generate a set of triangular elements  $K_j^*$  on the  $\Gamma_{\text{in}}$ .
2. Locate the vertices of the ghost element  $K_j$  by tracking the characteristics

$$(2.52) \quad \begin{cases} \frac{dx(t)}{dt} = a(x, y, t), \\ \frac{dy(t)}{dt} = b(x, y, t), \\ x(t^*) = x_{j,q}^*, \quad y(t^*) = y_{j,q}^*, \end{cases}$$

where  $(x_{j,q}^*, y_{j,q}^*, t^*)$  is the coordinates of the vertex of element  $K_j^*$ , as illustrated in Figure 2.3 (b). We denote the region which originates from  $K_j^*$  to  $K_j$  along the characteristics by  $\mathcal{K}$ . Note that the velocity field  $\mathbf{V}(x, y, t)$  outside of  $\Omega$  is the natural extension of the velocity field in  $\Omega$ .

3. We consider the adjoint problem for the test function  $\psi$ ,

$$(2.53) \quad \psi_t + \mathbf{V}(x, y, t) \cdot \nabla_{x,y} \psi = 0, \quad \psi(x, y, t = t^n) = \Psi(x, y) \in P^k(K_j).$$

Integrate (2.1)  $\cdot \psi$  + (2.53)  $\cdot u$  over  $\mathcal{K}$ , that is,

$$(2.54) \quad \int_{\mathcal{K}} [(\text{2.1}) \cdot \psi + (\text{2.6}) \cdot u] dx dy dt = 0.$$

After manipulating the above equation with the divergence theorem, we have

$$(2.55) \quad \int_{K_j} u \Psi dx dy = \int_{K_j^*} (\mathbf{V}(x, y, t) u \psi) \cdot \mathbf{n} dS,$$

where  $dS$  is infinitesimal of  $K_j^*$ . We adopt the SLDG scheme in [28, 31] to evaluate the R.H.S. of the above equation.

**3. Numerical results.** In this section, we demonstrate the performance of the proposed SLDG and EL-RKDG schemes for 2D transports equations, in terms of mass conservation, discrete geometric conservation law, high order accuracy in both space and time, numerical stability for large time stepping size as well as ability to capture discontinuities. In order to better show the advantages of the proposed schemes, we compare the results of the schemes with those of the classic RKDG method under the same settings. As in [35], the CFL number is defined by

$$(3.1) \quad CFL = \frac{\max_j \max_{\text{face}} |\mathbf{V} \cdot \mathbf{n}|}{\min_j R_j} \Delta t,$$

where  $R_j$  is the radius of the inscribed circle of the element  $K_j$  and  $\mathbf{n}$  is the unit normal vector of the face of  $K_j$ ;

$$(3.2) \quad R_j = 2 \frac{|K_j|}{|\partial K_j|},$$

where  $|K_j|$  and  $|\partial K_j|$  are the area and perimeter of  $K_j$ , respectively. By tests, we found there is little difference between the scheme with GCL correction and that without GCL correction besides the preservation capability. Thus unless otherwise noted, the EL-RKDG scheme for simulations is without GCL correction.

- *Mass conservation and discrete geometric conservation law.* For all simulations, we find that the mass is conserved up to machine precision for each time step of the presented schemes and we omit the results for brevity. The discrete GCL of EL-RKDG is verified in Example 3.2.
- *Consistency.* We test the spatial and temporal accuracy by linear transport problem, rotation and swirling deformation flow. For linear transport problem, we test the schemes for the problem with either periodic boundary conditions or inflow boundary conditions; the results are almost the same thus we only present the later in Example 3.1. For EL-RKDG, the expect high order accuracy can be observed for all these tests; for the proposed  $P^2$  SLDG, we observe the second order of convergence for solving the swirling deformation flow.

- *Stability.* The SLDG is numerical unconditional stable and EL-RKDG is numerically stable around time stepping size of  $\Delta t \sim \sqrt{h}$ , in Figures 3.3-3.5. The results are consistent with those in [10].
- *Resolution for discontinuities.* A simple WENO limiter in [59] used for all schemes is used to control oscillations for problems with discontinuities. Note that some advanced limiters such as [58] can be applied in the proposed schemes as well. We find the SLDG and EL-RKDG method can do a better job on the resolution of solutions around discontinuities, compared to RKDG.

EXAMPLE 3.1. (2D linear equation.) To verify the spatial accuracy of the EL-RKDG method with large time-stepping size, we apply the scheme to solve the following linear equation in two dimensions up to  $T = 1$ :

$$(3.3) \quad u_t + u_x + u_y = 0, \quad (x, y) \in [-\pi, \pi]^2$$

with the initial condition  $u(x, y, 0) = \sin(x + y)$  and the inflow boundary conditions,  $u(x = -\pi, y, t) = \sin(y - \pi - 2t)$  and  $u(x, y = -\pi, t) = \sin(x - \pi - 2t)$ . As shown in Figure 3.1, the structured uniform mesh and the unstructured mesh generated by the Gmsh [27] are used to test the mesh adaptability in this example. We report the

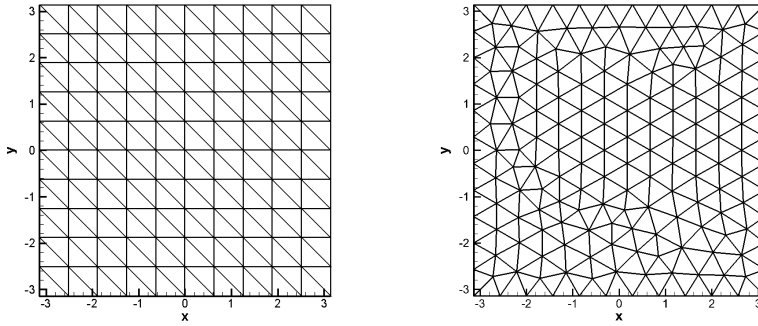


FIG. 3.1. Left: the structured triangular mesh,  $N = 2 \times 10^2$ . Right: the unstructured triangular mesh,  $N = 300$ .

$L^1$  errors and corresponding order of convergence of  $P^k$  ( $k = 1, 2$ ) EL-RKDG scheme with  $CFL = 10.2$  in Table 3.1. The expected  $k + 1$ -th orders of convergence are observed for  $P^k$  EL-RKDG scheme with either the structured uniform mesh or the unstructured mesh.

TABLE 3.1

$L^1$  errors of EL-RKDG schemes for linear problem,  $u_t + u_x + u_y = 0, (x, y) \in [-\pi, \pi]^2$  with the initial condition  $u(x, y, 0) = \sin(x + y)$  and the inflow boundary condition.  $T = 1$ .  $CFL = 10.2$ .

Structured triangular meshes				Unstructured triangular meshes					
	$P^1$ EL-RKDG	$P^2$ EL-RKDG			$P^1$ EL-RKDG	$P^2$ EL-RKDG			
Mesh	$L^1$ error	Order	$L^1$ error	Order	Mesh	$L^1$ error	Order	$L^1$ error	Order
$2 \times 20^2$	1.73E-03	—	7.67E-05	—	1018	2.31E-03	—	6.98E-05	—
$2 \times 40^2$	4.77E-04	1.85	8.51E-06	3.17	4132	5.47E-04	2.06	8.33E-06	3.04
$2 \times 80^2$	1.09E-04	2.12	1.02E-06	3.07	16364	1.43E-04	1.95	9.24E-07	3.19
$2 \times 160^2$	2.72E-05	2.01	1.01E-07	3.33	65278	3.75E-05	1.94	1.54E-07	2.59

EXAMPLE 3.2. (*The GCL property.*) To verify the GCL property of the EL-RKDG method, we test the previous example with the conditions  $u(x, y, 0) = 1$ ,  $u(x = -\pi, y, t) = 1$ ,  $u(x, y = -\pi, t) = 1$ . In the result of Proposition 2.7, the GCL property of the EL-RKDG scheme relies on the time integration; we test  $P^1$  EL-RKDG scheme with SSP-RK2 and SSP-RK3, using  $CFL = 10.2$ , in which the velocity field is perturbed by a random number multiplying  $h$ . The results of the EL-RKDG scheme with either discrete GCL or without discrete GCL are listed in Table 3.2. We observe that: the EL-RKDG scheme without discrete GCL approximates the constant solutions in the high order accuracy; yet the EL-RKDG scheme with discrete GCL exactly preserves the GCL property.

TABLE 3.2

GCL tests on the linear problem,  $u_t + u_x + u_y = 0, (x, y) \in [-\pi, \pi]^2$  with the initial condition  $u(x, y, 0) = 1$ ,  $u(x = -\pi, y, t) = 1$ ,  $u(x, y = -\pi, t) = 1$  at  $T = 1$ .  $P^1$  EL-RKDG scheme with different temporal methods, using  $CFL = 10.2$ , in which the velocity field is perturbed randomly. The EL-RKDG scheme with discrete GCL (GCL), without discrete GCL (no GCL).

Mesh	no GCL				GCL			
	SSP-RK2		SSP-RK3		SSP-RK2		SSP-RK3	
	$L^2$ error	Order		$L^2$ error	Order		$L^2$ error	Order
1018	1.95E-05	–	7.64E-07	–	1.11E-13	–	1.11E-13	–
4132	1.17E-06	4.01	1.45E-08	5.66	2.19E-13	–	2.18E-13	–
16364	2.72E-07	2.12	2.42E-09	2.60	3.61E-13	–	3.61E-13	–
65278	2.23E-08	3.61	7.18E-11	5.09	7.75E-13	–	7.73E-13	–

EXAMPLE 3.3. (*Rigid body rotation on a circle domain.*) Consider

$$(3.4) \quad u_t - (yu)_x + (xu)_y = 0, \quad (x, y) \in \{(x, y) | x^2 + y^2 \leq \pi^2\}$$

with the initial condition  $u(x, y, 0) = \exp(-3x^2 - 3y^2)$ . The coarsest mesh  $N = 160$  is shown in Figure 3.2.

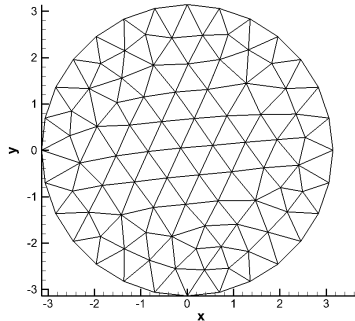


FIG. 3.2. The unstructured mesh with the mesh of 160 is generated by GMSH.

First, we test the spatial convergence of the proposed SLDG schemes, proposed EL-RKDG schemes, and the RKDG schemes. We use the same time-stepping sizes for comparison; the CFL numbers in time step selection are set to be 0.3 for  $P^1$  DG and 0.15 for  $P^2$  DG. These time-stepping sizes are with the stability constraint of  $1/(2k + 1)$  for RKDG. We summarize the results of these scheme for solving the

problem up to  $T = 2\pi$  in Table 3.3. We observe the expected orders of convergence and the similar results for different DG schemes.

Second, we study numerical stabilities of EL-RKDG and SLDG schemes. We present the plots of  $L^1$  error versus CFL of these schemes in Figure 3.3. We make a few observations: (1) When CFL is relatively large but smaller than the stability constraint of EL-RKDG, the temporal errors starting to kick in 2nd and 3rd order temporal convergence order are shown. (2) Maximum CFLs with numerical stability of  $P^2$  EL-RKDG using meshes  $N = 1884, 7432, 28996$  are 13.8, 19.6, 27.5, respectively. The increasing rate is around  $\sqrt{2}$ . (3) SLDG schemes are stable for arbitrarily large time-stepping sizes.

Third, we numerically solve the rigid body rotation (3.4) with an initial condition plotted in Figure 3.4 (a), which consists of a slotted disk, a cone as well as a smooth hump, similar to the one used in [33] for comparison purposes. In Figure 3.4, we present plots of the solutions solved by  $P^2$  RKDG, SLDG, and EL-RKDG schemes with WENO limiter after one full rotation. We use  $CFL=10.2$  for SLDG and EL-RKDG. We observe that: (1) the solutions of SLDG and EL-RKDG are comparable; (2) the solutions of SLDG and EL-RKDG are less dissipative than that of RKDG, due to the fewer error accumulations of the schemes with large time-stepping size.

TABLE 3.3

Errors of different DG schemes for rigid body rotation on a circle domain with the initial condition  $u(x, y, 0) = \exp(-3x^2 - 3y^2)$ .  $T = 2\pi$ . The  $CFL=0.3$  for  $P^1$  DG and  $CFL=0.15$  for  $P^2$  DG.

Mesh	$L^1$ error	Order	$L^1$ error	Order	$L^1$ error	Order
	$P^1$ EL-RKDG		$P^1$ SLDG		$P^1$ RKDG	
522	2.37E-03	—	2.37E-03	—	2.40E-03	—
1884	5.24E-04	2.35	5.24E-04	2.35	5.33E-04	2.35
7432	1.15E-04	2.21	1.15E-04	2.21	1.17E-04	2.21
28996	2.77E-05	2.09	2.77E-05	2.09	2.81E-05	2.10
	$P^2$ EL-RKDG		$P^2$ SLDG		$P^2$ RKDG	
	1.88E-04	—	1.89E-04	—	1.94E-04	—
1884	2.41E-05	3.20	2.41E-05	3.21	2.43E-05	3.24
7432	2.91E-06	3.08	2.91E-06	3.08	2.94E-06	3.08
28996	3.62E-07	3.07	3.62E-07	3.07	3.65E-07	3.07

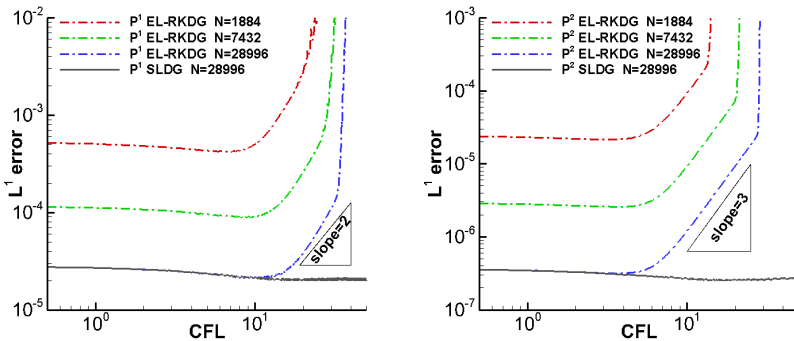


FIG. 3.3. The  $L^1$  error versus CFL of SLDG schemes and EL-RKDG schemes for the rigid body rotation with  $u(x, y, 0) = \exp(-3x^2 - 3y^2)$ .  $T = 2\pi$ .

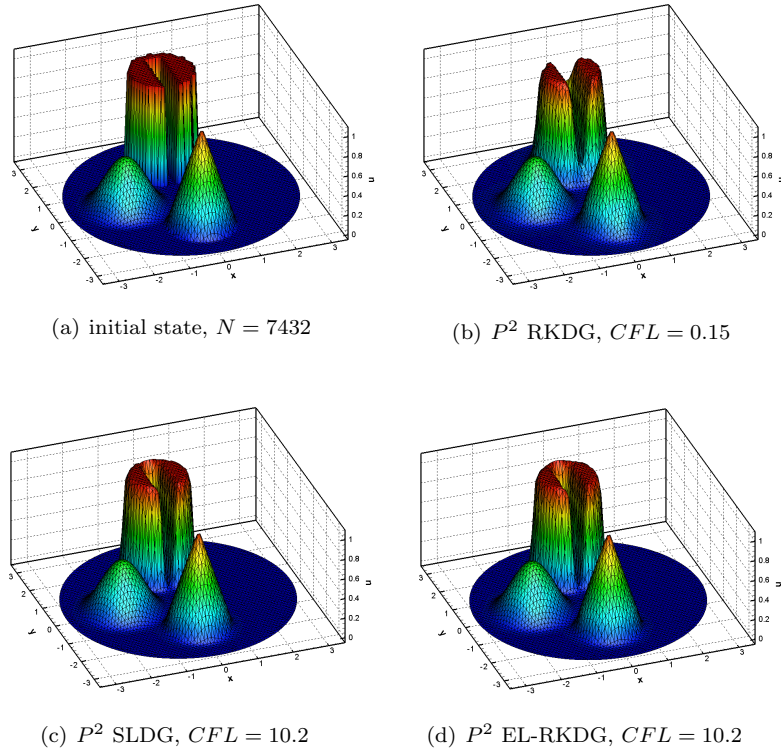


FIG. 3.4. Plots of the numerical solutions of  $P^2$  SLDG and EL-RKDG schemes the rigid body rotation with the initial condition in (a).  $T = 2\pi$ .

EXAMPLE 3.4. (Swirling deformation flow.) We consider solving

$$(3.5) \quad u_t - \left( \cos^2 \left( \frac{x}{2} \right) \sin(y) g(t) u \right)_x + \left( \sin(x) \cos^2 \left( \frac{y}{2} \right) g(t) u \right)_y = 0, \quad (x, y) \in [-\pi, \pi]^2,$$

where  $g(t) = \cos \left( \frac{\pi t}{T} \right) \pi$  and  $T = 1.5$ . The initial condition is set to be the following smooth cosine bell (with  $C^5$  smoothness),

$$(3.6) \quad u(x, y, 0) = \begin{cases} r_0^b \cos^6 \left( \frac{r^b}{2r_0^b} \pi \right), & \text{if } r^b < r_0^b, \\ 0, & \text{otherwise,} \end{cases}$$

where  $r_0^b = 0.3\pi$ , and  $r^b = \sqrt{(x - x_0^b)^2 + (y - y_0^b)^2}$  denotes the distance between  $(x, y)$  and the center of the cosine bell  $(x_0^b, y_0^b) = (0.3\pi, 0)$ . As Example 3.3, we study the spatial error and the numerical stability of the proposed SLDG and EL-RKDG schemes in Table 3.4 and Figure 3.5, respectively. The similar observations as Example 3.3 can be made for  $P^1$  part. We find that  $P^2$  SLDG is of second order due to the second approximation to the sides of upstream cells while  $P^2$  EL-RKDG is of third order. Figure 3.6 presents spatial errors and CPU times of EL-RKDG method and SLDG method; we observe that with the same setting, SLDG is more expensive in CPU time to achieve the same error, compared to EL-RKDG.

TABLE 3.4

Errors of different DG schemes for swirling deformation flow with the smooth cosine bell.  $T = 1.5$ .  $CFL = 0.3$  and  $0.15$  for  $P^1$  and  $P^2$ , respectively.

Mesh	$L^1$ error	Order	$L^1$ error	Order	$L^1$ error	Order
	$P^1$ EL-RKDG		$P^1$ SLDG		$P^1$ RKDG	
$2 \times 20^2$	2.97E-03	—	2.91E-03	—	3.07E-03	—
$2 \times 40^2$	7.18E-04	2.05	7.05E-04	2.05	7.64E-04	2.01
$2 \times 80^2$	1.28E-04	2.49	1.26E-04	2.49	1.37E-04	2.48
$2 \times 160^2$	2.25E-05	2.50	2.22E-05	2.50	2.39E-05	2.50
	$P^2$ EL-RKDG		$P^2$ SLDG		$P^2$ RKDG	
	4.90E-04	—	4.77E-04	—	5.10E-04	—
$2 \times 20^2$	3.88E-05	3.66	4.27E-05	3.48	4.03E-05	3.66
$2 \times 40^2$	3.41E-06	3.51	5.99E-06	2.83	3.51E-06	3.52
$2 \times 80^2$	3.77E-07	3.18	1.26E-06	2.25	3.90E-07	3.17

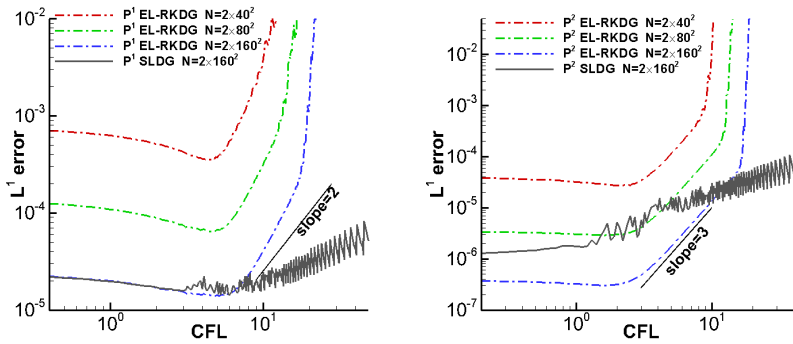


FIG. 3.5. The  $L^1$  error versus  $CFL$  of SLDG schemes and EL-RKDG schemes for the swirling deformation flow with the smooth cosine bell.  $T = 1.5$ .

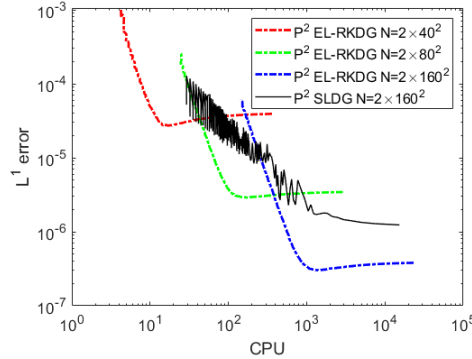


FIG. 3.6. The  $L^1$  error versus CPU time of SLDG schemes and EL-RKDG schemes for the swirling deformation flow with the smooth cosine bell.  $T = 1.5$ .

As Example 3.3, we numerically solve the swirling deformation flow (3.5) with an initial condition plotted in Figure 3.7 (a). The results are present in Figure 3.7. The similar observations as Example 3.3 can be made.

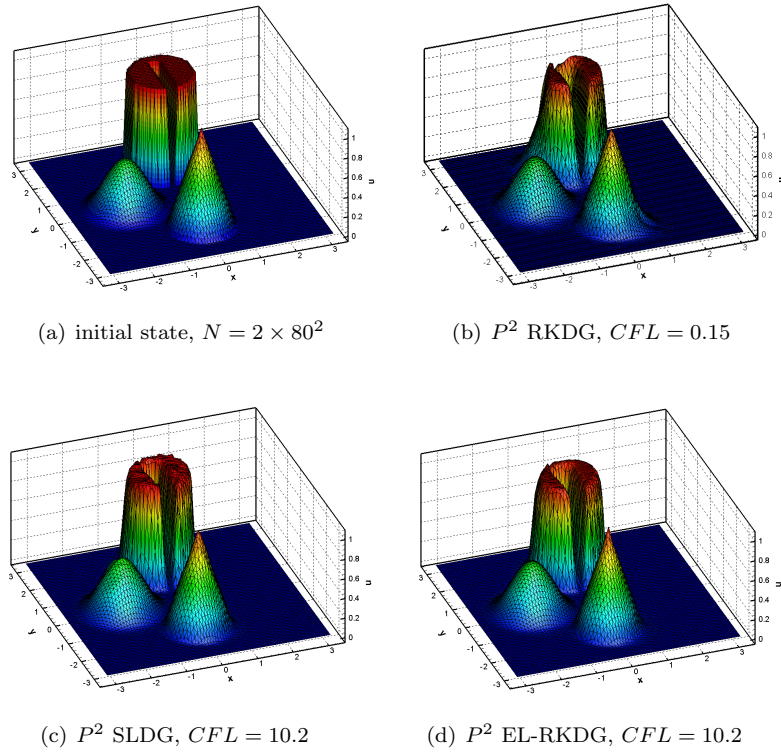


FIG. 3.7. Plots of the numerical solutions of  $P^2$  SLDG and EL-RKDG schemes the swirling deformation flow with the initial condition in (a).  $T = 1.5$ .  $N = 2 \times 80^2$

**4. Conclusion.** We have devised the SLDG method and the EL-RKDG method on the unstructured triangular meshes for linear transport problems. The crucial ingredient of the present schemes is the conservative remapping algorithm. Then the proposed schemes can be mass conservative. To the best of our knowledge, the present SLDG scheme is the first SL scheme on the unstructured mesh that can enjoy favorable properties of mass conservation, second-order accuracy, and unconditionally numerical stability; the present EL-RKDG can inherit main favourable properties and can largely alleviate the CFL constraint from RKDG. The theoretical analysis of the stability of the present schemes is subject to our future investigation.

This is an initial effort to propose accurate and conservative semi-Lagrangian schemes for the practical problems with complex geometry. Although the presented schemes are just for linear transport problems, we believe they can be extended to nonlinear transport problems via exponential integrators in [7], which has successfully coupled with the SLDG method on the structured meshes. And we believe it can also be extended for convection-diffusion equations, as in [19]. These extensions will be investigated in our future research work. As we mentioned, the semi-Lagrangian schemes are popular in the climate modeling and kinetic models. Hence, it would be interesting to use this solver for these applications.

#### REFERENCES

- [1] F. ALAUZET, *A parallel matrix-free conservative solution interpolation on unstructured tetrahedral meshes*, Computer Methods in Applied Mechanics and Engineering, 299 (2016), pp. 116–142.
- [2] F. ALAUZET AND M. MEHRENBERGER, *P1-conservative solution interpolation on unstructured triangular meshes*, International Journal for Numerical Methods in Engineering, 84 (2010), pp. 1552–1588.
- [3] N. BESSE, J. SEGRÉ, AND E. SONNENDRÜCKER, *Semi-Lagrangian Schemes for the Two-Dimensional Vlasov-Poisson System on Unstructured Meshes*, Transport Theory and Statistical Physics, 34 (2005), pp. 311–332.
- [4] N. BESSE AND E. SONNENDRÜCKER, *Semi-Lagrangian schemes for the Vlasov equation on an unstructured mesh of phase space*, Journal of Computational Physics, 191 (2003), pp. 341–376.
- [5] O. BOKANOWSKI AND G. SIMARMATA, *Semi-Lagrangian discontinuous Galerkin schemes for some first-and second-order partial differential equations*, ESAIM: Mathematical Modelling and Numerical Analysis, 50 (2016), pp. 1699–1730.
- [6] P. A. BOSLER, A. M. BRADLEY, AND M. A. TAYLOR, *Conservative Multimoment Transport along Characteristics for Discontinuous Galerkin Methods*, SIAM Journal on Scientific Computing, 41 (2019), pp. B870–B902.
- [7] X. CAI, S. BOSCARINO, AND J.-M. QIU, *High order semi-Lagrangian discontinuous Galerkin method coupled with Runge-Kutta exponential integrators for nonlinear Vlasov dynamics*, Journal of Computational Physics, 427 (2021), p. 110036.
- [8] X. CAI, W. GUO, AND J.-M. QIU, *A high order conservative semi-Lagrangian discontinuous Galerkin method for two-dimensional transport simulations*, Journal of Scientific Computing, 73 (2017), pp. 514–542.
- [9] X. CAI, W. GUO, AND J.-M. QIU, *A high order semi-Lagrangian discontinuous Galerkin method for Vlasov-Poisson simulations without operator splitting*, Journal of Computational Physics, 354 (2018), pp. 529–551.
- [10] X. CAI, J.-M. QIU, AND Y. YANG, *An Eulerian-Lagrangian discontinuous Galerkin method for transport problems and its application to nonlinear dynamics*, Journal of Computational Physics, 439 (2021), p. 110392.
- [11] M. A. CELIA, T. F. RUSSELL, I. HERRERA, AND R. E. EWING, *An Eulerian-Lagrangian localized adjoint method for the advection-diffusion equation*, Advances in water resources, 13 (1990), pp. 187–206.
- [12] N. CHALMERS AND L. KRIVODONOVA, *A robust CFL condition for the discontinuous Galerkin method on triangular meshes*, Journal of Computational Physics, 403 (2020), p. 109095.
- [13] J. CHENG AND C.-W. SHU, *A high order accurate conservative remapping method on staggered meshes*, Applied Numerical Mathematics, 58 (2008), pp. 1042–1060.
- [14] Y. CHENG, I. GAMBA, F. LI, AND P. MORRISON, *Discontinuous Galerkin methods for the Vlasov-Maxwell equations*, SIAM Journal on Numerical Analysis, 52 (2014), pp. 1017–1049.
- [15] P. G. CIARLET, *Mathematical Elasticity: Volume I: three-dimensional elasticity*, North-Holland, 1988.
- [16] B. COCKBURN AND C.-W. SHU, *Runge-Kutta discontinuous Galerkin methods for convection-dominated problems*, Journal of Scientific Computing, 16 (2001), pp. 173–261.
- [17] N. CROUSEILLES, P. GLANC, S. A. HIRSTOAGA, E. MADAULE, M. MEHRENBERGER, AND J. PÉTRI, *A new fully two-dimensional conservative semi-Lagrangian method: applications on polar grids, from diocotron instability to ITG turbulence*, The European Physical Journal D, 68 (2014), pp. 1–10.
- [18] N. CROUSEILLES, M. MEHRENBERGER, AND F. VECIL, *Discontinuous Galerkin semi-Lagrangian method for Vlasov-Poisson*, in ESAIM: Proceedings, vol. 32, EDP Sciences, 2011, pp. 211–230.
- [19] M. DING, X. CAI, W. GUO, AND J.-M. QIU, *A semi-Lagrangian discontinuous Galerkin (DG) – local DG method for solving convection-diffusion equations*, Journal of Computational Physics, 409 (2020), p. 109295.
- [20] J. DOUGLAS JR AND T. RUSSELL, *Numerical methods for convection-dominated diffusion problems based on combining the method of characteristics with finite element or finite difference procedures*, SIAM Journal on Numerical Analysis, 19 (1982), pp. 871–885.
- [21] D. DUNAVANT, *High degree efficient symmetrical Gaussian quadrature rules for the triangle*, International journal for numerical methods in engineering, 21 (1985), pp. 1129–1148.
- [22] P. FARRELL AND J. MADDISON, *Conservative interpolation between volume meshes by local Galerkin projection*, Computer Methods in Applied Mechanics and Engineering, 200 (2011), pp. 89–100.

- [23] P. E. FARRELL, M. D. PIGGOTT, C. C. PAIN, G. J. GORMAN, AND C. R. WILSON, *Conservative interpolation between unstructured meshes via supermesh construction*, Computer methods in applied mechanics and engineering, 198 (2009), pp. 2632–2642.
- [24] F. FILBET, E. SONNENDRÜCKER, AND P. BERTRAND, *Conservative numerical schemes for the Vlasov equation*, Journal of Computational Physics, 172 (2001), pp. 166–187.
- [25] L. FORMAGGIA AND F. NOBILE, *Stability analysis of second-order time accurate schemes for ALE-FEM*, Computer methods in applied mechanics and engineering, 193 (2004), pp. 4097–4116.
- [26] P. FU, G. SCHNÜCKE, AND Y. XIA, *Arbitrary Lagrangian-Eulerian discontinuous Galerkin method for conservation laws on moving simplex meshes*, Mathematics of Computation, 88 (2019), pp. 2221–2255.
- [27] C. GEUZAINIE AND J.-F. REMACLE, *Gmsh: A 3-D finite element mesh generator with built-in pre-and post-processing facilities*, International Journal for Numerical Methods in Engineering, 79 (2009), pp. 1309–1331.
- [28] W. GUO, R. NAIR, AND J.-M. QIU, *A conservative semi-Lagrangian discontinuous Galerkin scheme on the cubed-sphere*, Monthly Weather Review, 142 (2013), pp. 457–475.
- [29] C.-S. HUANG, T. ARBOGAST, AND C.-H. HUNG, *A semi-Lagrangian finite difference WENO scheme for scalar nonlinear conservation laws*, Journal of Computational Physics, 322 (2016), pp. 559–585.
- [30] P. LAURITZEN, R. NAIR, AND P. ULLRICH, *A conservative semi-Lagrangian multi-tracer transport scheme (CSLAM) on the cubed-sphere grid*, Journal of Computational Physics, 229 (2010), pp. 1401–1424.
- [31] D. LEE, R. LOWRIE, M. PETERSEN, T. RINGLER, AND M. HECHT, *A high order characteristic discontinuous Galerkin scheme for advection on unstructured meshes*, Journal of Computational Physics, 324 (2016), pp. 289–302.
- [32] T. LEE AND C. LIN, *A characteristic Galerkin method for discrete Boltzmann equation*, Journal of Computational Physics, 171 (2001), pp. 336–356.
- [33] R. LEVEQUE, *High-resolution conservative algorithms for advection in incompressible flow*, SIAM Journal on Numerical Analysis, 33 (1996), pp. 627–665.
- [34] H. LIU, X. CAI, G. LAPENTA, AND Y. CAO, *Conservative semi-Lagrangian kinetic scheme coupled with implicit finite element field solver for multidimensional Vlasov Maxwell system*, Communications in Nonlinear Science and Numerical Simulation, 102 (2021), p. 105941.
- [35] D. LUO, W. HUANG, AND J. QIU, *A quasi-Lagrangian moving mesh discontinuous Galerkin method for hyperbolic conservation laws*, Journal of Computational Physics, 396 (2019), pp. 544–578.
- [36] K. MORTON, A. PRIESTLEY, AND E. SULI, *Stability of the Lagrange-Galerkin method with non-exact integration*, ESAIM: Mathematical Modelling and Numerical Analysis, 22 (1988), pp. 625–653.
- [37] K. W. MORTON, *On the analysis of finite volume methods for evolutionary problems*, SIAM journal on numerical analysis, 35 (1998), pp. 2195–2222.
- [38] P.-O. PERSSON, J. BONET, AND J. PERAIRE, *Discontinuous Galerkin solution of the Navier-Stokes equations on deformable domains*, Computer Methods in Applied Mechanics and Engineering, 198 (2009), pp. 1585–1595.
- [39] O. PIRONNEAU, *On the transport-diffusion algorithm and its applications to the Navier-Stokes equations*, Numerische Mathematik, 38 (1982), pp. 309–332.
- [40] J.-M. QIU AND C.-W. SHU, *Conservative high order semi-Lagrangian finite difference WENO methods for advection in incompressible flow*, Journal of Computational Physics, 230 (2011), pp. 863–889.
- [41] M. RESTELLI, L. BONAVENTURA, AND R. SACCO, *A semi-Lagrangian discontinuous Galerkin method for scalar advection by incompressible flows*, Journal of Computational Physics, 216 (2006), pp. 195–215.
- [42] B. RIVIERE, *Discontinuous Galerkin methods for solving elliptic and parabolic equations: theory and implementation*, SIAM, 2008.
- [43] J. A. ROSSMANITH AND D. C. SEAL, *A positivity-preserving high-order semi-Lagrangian discontinuous Galerkin scheme for the Vlasov-Poisson equations*, Journal of Computational Physics, 230 (2011), pp. 6203–6232.
- [44] T. RUSSELL AND M. CELIA, *An overview of research on Eulerian-Lagrangian localized adjoint methods (ELLAM)*, Advances in Water Resources, 25 (2002), pp. 1215–1231.
- [45] C.-W. SHU AND S. OSHER, *Efficient implementation of essentially non-oscillatory shock-capturing schemes*, Journal of Computational Physics, 77 (1988), pp. 439–471.
- [46] Z. SI, J. WANG, AND W. SUN, *Unconditional stability and error estimates of modified characteristics FEMs for the Navier-Stokes equations*, Numerische Mathematik, 134 (2016),

pp. 139–161.

[47] I. E. SUTHERLAND AND G. W. HODGMAN, *Reentrant polygon clipping*, Communications of the ACM, 17 (1974), pp. 32–42.

[48] Z. TAO, W. GUO, AND Y. CHENG, *Sparse grid discontinuous Galerkin methods for the Vlasov-Maxwell system*, Journal of Computational Physics: X, 3 (2019), p. 100022.

[49] P. D. THOMAS AND C. K. LOMBARD, *Geometric conservation law and its application to flow computations on moving grids*, AIAA journal, 17 (1979), pp. 1030–1037.

[50] S. TIRUPATHI, J. S. HESTHAVEN, Y. LIANG, AND M. PARMENTIER, *Multilevel and local time-stepping discontinuous Galerkin methods for magma dynamics*, Computational Geosciences, 19 (2015), pp. 965–978.

[51] J. G. TRULIO AND K. R. TRIGGER, *Numerical solution of the one-dimensional hydrodynamic equations in an arbitrary time-dependent coordinate system*, University of California Lawrence Radiation Laboratory Report UCLR-6522, (1961).

[52] H. WANG, R. EWING, G. QIN, S. LYONS, M. AL-LAWATIA, AND S. MAN, *A family of Eulerian-Lagrangian localized adjoint methods for multi-dimensional advection-reaction equations*, Journal of Computational Physics, 152 (1999), pp. 120–163.

[53] J. WANG, Z. SI, AND W. SUN, *A new error analysis of characteristics-mixed FEMs for miscible displacement in porous media*, SIAM Journal on Numerical Analysis, 52 (2014), pp. 3000–3020.

[54] Y. YANG, X. CAI, AND J.-M. QIU, *Optimal convergence and superconvergence of semi-Lagrangian discontinuous Galerkin methods for linear convection equations in one space dimension*, Mathematics of Computation, 89 (2020), pp. 2113–2139.

[55] A. YOUNES, P. ACKERER, AND F. LEHMANN, *A new efficient Eulerian-Lagrangian localized adjoint method for solving the advection-dispersion equation on unstructured meshes*, Advances in water resources, 29 (2006), pp. 1056–1074.

[56] M. ZHANG, W. HUANG, AND J. QIU, *High-order conservative positivity-preserving DG-interpolation for deforming meshes and application to moving mesh DG simulation of radiative transfer*, SIAM Journal on Scientific Computing, 42 (2020), pp. A3109–A3135.

[57] X. ZHANG, *On positivity-preserving high order discontinuous Galerkin schemes for compressible Navier-Stokes equations*, Journal of Computational Physics, 328 (2017), pp. 301–343.

[58] J. ZHU, C.-W. SHU, AND J. QIU, *High-order Runge-Kutta discontinuous Galerkin methods with a new type of multi-resolution WENO limiters on triangular meshes*, Applied Numerical Mathematics, 153 (2020), pp. 519–539.

[59] J. ZHU, X. ZHONG, C.-W. SHU, AND J. QIU, *Runge-Kutta discontinuous Galerkin method using a new type of WENO limiters on unstructured meshes*, Journal of Computational Physics, 248 (2013), pp. 200–220.